


## Article

# Embedding Group VIII Elements into a 2D Rigid pc-C<sub>3</sub>N<sub>2</sub> Monolayer to Achieve Single-Atom Catalysts with Excellent OER Activity: A DFT Theoretical Study

Qingxian Wang <sup>1</sup>, E Yang <sup>1</sup>, Ran Liu <sup>1</sup>, Mingyue Lv <sup>1</sup>, Wei Zhang <sup>2,3,\*</sup>, Guangtao Yu <sup>1,\*</sup> and Wei Chen <sup>1,2,4,\*</sup> 

<sup>1</sup> Engineering Research Center of Industrial Biocatalysis, Fujian Provincial Key Laboratory of Advanced Materials Oriented Chemical Engineering, Fujian-Taiwan Science and Technology Cooperation Base of Biomedical Materials and Tissue Engineering, College of Chemistry and Materials Science, Fujian Normal University, Fuzhou 350007, China

<sup>2</sup> Academy of Carbon Neutrality of Fujian Normal University, Fuzhou 350007, China

<sup>3</sup> Fujian Provincial Key Laboratory of Quantum Manipulation and New Energy Materials, College of Physics and Energy, Fujian Normal University, Fuzhou 350117, China

<sup>4</sup> Fujian Provincial Key Laboratory of Theoretical and Computational Chemistry, Xiamen University, Xiamen 361005, China

\* Correspondence: zhangwei@fjnu.edu.cn (W.Z.); yugt@fjnu.edu.cn (G.Y.); chenwei@fjnu.edu.cn (W.C.)

**Abstract:** Under DFT calculations, a systematic investigation is carried out to explore the structures and oxygen evolution reaction (OER) catalytic activities of a series of 2D single-atom catalyst (SAC) systems, which are constructed by doping the transition metal (TM) atoms in group VIII into the cavities of rigid phthalocyanine carbide (pc-C<sub>3</sub>N<sub>2</sub>). We can find that when Co, Rh, Ir and Ru atoms are doped in the small or large cavities of a pc-C<sub>3</sub>N<sub>2</sub> monolayer, they can be used as high-activity centers of OER. All these four new TM@C<sub>3</sub>N<sub>2</sub> nanostructures can exhibit very low overpotential values in the range of 0.33~0.48 V, even smaller than the state-of-the-art IrO<sub>2</sub> (0.56 V), which indicates considerably high OER catalytic activity. In particular, the Rh@C<sub>3</sub>N<sub>2</sub> system can show the best OER performance, given that doped Rh atoms can uniformly serve as high-OER-active centers, regardless of the size of cavity. In addition, a detailed mechanism analysis was carried out. It is found that in these doped pc-C<sub>3</sub>N<sub>2</sub> systems, the number of outer electrons, the periodic number of doped TM atoms and the size of the embedded cavity can be considered the key factors affecting the OER catalytic activity, and excellent OER catalytic performance can be achieved through their effective cooperation. These fascinating findings can be advantageous for realizing low-cost and high-performance SAC catalysts for OER in the near future.

**Keywords:** single-atom catalyst (SAC); oxygen evolution reaction (OER); electrocatalyst; 2D pc-C<sub>3</sub>N<sub>2</sub> monolayer; DFT calculations



**Citation:** Wang, Q.; Yang, E.; Liu, R.; Lv, M.; Zhang, W.; Yu, G.; Chen, W. Embedding Group VIII Elements into a 2D Rigid pc-C<sub>3</sub>N<sub>2</sub> Monolayer to Achieve Single-Atom Catalysts with Excellent OER Activity: A DFT Theoretical Study. *Molecules* **2023**, *28*, 254. <https://doi.org/10.3390/molecules28010254>

Academic Editor: Carlo Santoro

Received: 15 November 2022

Revised: 19 December 2022

Accepted: 23 December 2022

Published: 28 December 2022



**Copyright:** © 2022 by the authors. Licensee MDPI, Basel, Switzerland. This article is an open access article distributed under the terms and conditions of the Creative Commons Attribution (CC BY) license (<https://creativecommons.org/licenses/by/4.0/>).

## 1. Introduction

Since the 21st century, the environmental and energy crisis has become increasingly serious. Developing new clean energy sources can be regarded as an effective strategy to alleviate this major problem [1,2]. Some obvious advantages of hydrogen energy, such as rich reserves and the lack of pollution to the environment after combustion, make it one of the most promising energy carriers [3,4]. The electrocatalytic splitting of the most abundant water on the earth has been considered to be the most efficient and sustainable hydrogen production method [5,6]. It is well known that the oxygen evolution reaction (OER) at the anode, as one half-reaction of water splitting, involves a complex four-electron transfer process, and it is kinetically slow and is usually the rate-determining step [7,8]. Both IrO<sub>2</sub> and RuO<sub>2</sub> materials are recognized as the most efficient OER catalysts [9,10]. However, they cannot be widely used due to their high cost and low abundance. Therefore, it is urgent to find some alternative, efficient and sustainable OER catalyst.

Different strategies have been proposed to design efficient OER catalysts, mainly by reducing the content of precious metals and developing nonprecious metal alternatives [11–19]. With the development of synthetic technologies, the emergence of single-atom catalytic materials has promising prospects for achieving nonprecious and highly active OER catalysts. Compared with the traditional catalysts, single-atom catalysts (SACs) have shown great potential advantages, including high selectivity [20,21], tunable high activity [22] and maximum atomic efficiency [23]. At present, more and more attention has been paid to the design of efficient SAC catalysts for OER. For example, Zhang et al. found that inserting a Ni atom into a defect-rich graphene can achieve an SAC catalyst with good OER activity [24]. Lin et al. also reported that a SAC catalyst with high OER activity can be synthesized by anchoring Pt atoms on a metal oxide NiO nanotube [25]. Moreover, Chen et al. explored the OER catalytic activity of a series of monoatomic transition metals supported by the MXenes  $M_2NO_2$  ( $M = Ti, V$  and  $Cr$ ) through first principle calculations and found that a Cu-anchored  $Ti_2NO_2$  system can be used as an efficient SAC catalyst for OER [26]. Obviously, some different supports have been used to construct high-efficiency SAC catalysts, and the selection of appropriate support can play a crucial role in determining the high OER catalytic activity.

Different from the previous investigations, in this study, we mainly focus on a two-dimensional (2D)  $pc-C_3N_2$  monolayer containing two different cavities [27], which are surrounded by four N atoms in pyrrole-like units or four N atoms connecting the pyrrole-like units. This kind of unique porous structure with two different sizes of holes can be advantageous for trapping TM atoms with different atomic radii to form two different series of  $TMN_4$  centers in  $pc-C_3N_2$ , exhibiting promising OER catalytic activity. Besides, the high stability and excellent conductivity of a  $pc-C_3N_2$  monolayer [28] can also be conducive to its development as a suitable support for constructing potential SAC structures.

In this work, the TM atoms ( $TM = Fe, Co, Ni, Ru, Rh, Pd, Os, Ir$  and  $Pt$ ) in group VIII are embedded into the cavities of a fascinating carbon–nitrogen substrate  $pc-C_3N_2$  to construct a series of new  $TM@pc-C_3N_2$  structures with  $TMN_4$  centers. It is highly anticipated that some of these structures can exhibit considerably high OER catalytic performance. Herein, we have carried out systematic first-principles calculations to investigate their structures, electronic properties and OER catalytic activities. The following issues will be mainly addressed: (i) Does the introduction of these TM atoms of group VIII enhance the conductivity of these systems? (ii) Which TM atoms can be embedded to form SAC catalysts with high OER activity? (iii) How do the number of outer electrons and the periodic number of TM atoms affect the OER catalytic activity? (iv) Does the hole size have any effect on the OER catalytic performance? The solution of these problems will facilitate the design of new SAC catalysts with high OER catalytic performance based on the relevant systems with rigid framework, including  $pc-C_3N_2$ .

It is worth mentioning that our calculation results reveal that a series of new 2D structures with high stability and excellent conductivity can be obtained by doping these group VIII TM atoms into a porous  $pc-C_3N_2$  monolayer. Among them,  $pc-C_3N_2$  systems doped with Co, Rh, Ir and Ru atoms can uniformly exhibit a very low overpotential value in the range of 0.33–0.48 V, even smaller than the state-of-the-art  $IrO_2$  (0.56 V), which indicates the considerably high OER catalytic activity. This is the result of the combined effect of the number of outer electrons, the periodic number of doped TM atoms and the size of the embedded cavity.

## 2. Calculation Method

All the DFT calculations were performed by using the Vienna Ab initio Simulation Package (VASP) code [29]. The projector augmented wave (PAW) method [30–32] was used to describe the ion–electron interaction. The electronic exchange–correlation was approximated by the Perdew–Burke–Ernzerhof (PBE) functional in the generalized gradient approximation (GGA) [33], which includes the semiempirical van der Waals (vdW) method proposed by Grimme to correct for the dispersion interactions [29,34,35]. The kinetic cutoff

energy was set to 450 eV to truncate the plane wave basis. The Brillouin zone was sampled using the Monkhorst–Pack scheme [36] with  $3 \times 3 \times 1$  k-meshes for structure relaxation. A 20 Å vacuum along the z-direction was utilized to prevent spurious interaction between the periodically repeated images. The convergence thresholds for energy and atomic force components were set to  $10^{-4}$  eV and 0.05 eV/Å, respectively. It is worth mentioning that the obtained overpotentials can be very close to the corresponding ones from considering the solvent effect through VASPsol with a dielectric constant of 80, as revealed by our computational test on Ir@C<sub>3</sub>N<sub>2</sub> (Figure S1). This indicates that the solvent effect can have a negligible influence. Therefore, to make the computational cost less demanding, in this study, we performed correlative calculations in a vacuum condition for estimating the OER catalytic activity for the studied systems. In addition, we also performed a DFT+U computational test on a 3d metal-doped pc-C<sub>3</sub>N<sub>2</sub> system by sampling Co@C<sub>3</sub>N<sub>2</sub> (Figure S2), where the Hubbard U parameters of  $U_{\text{eff}} = U - J = 3.1$  eV ( $U = 4.0$  eV and  $J = 0.9$  eV) were adopted, according to previous work [37]. As shown in Figure S2, the OER overpotentials obtained by the DFT+U method can be comparable to the corresponding overpotentials calculated by DFT without U, indicating that all the present DFT results in this work can effectively evaluate the OER catalytic activity of relevant systems.

To estimate the stability, the binding energy of TM@pc-C<sub>3</sub>N<sub>2</sub> was calculated using the following formula:

$$E_b = E_{\text{pc-C}_3\text{N}_2} + nE_{\text{TM}} - E_{\text{TM@pc-C}_3\text{N}_2} \quad (1)$$

where  $E_{\text{TM@pc-C}_3\text{N}_2}$  and  $E_{\text{pc-C}_3\text{N}_2}$  are the total energies of TM@pc-C<sub>3</sub>N<sub>2</sub> and pristine pc-C<sub>3</sub>N<sub>2</sub>, respectively;  $n$  is the number of doped transition metal atoms;  $E_{\text{TM}}$  is the energy of an isolated TM atom.

The cohesive energy ( $E_c$ ) of a crystal is defined as the energy that must be added to the crystal to separate its components into neutral free atoms. The  $E_c$  value can be calculated by the following formula:

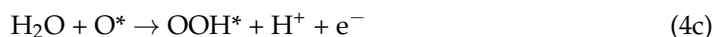
$$E_c = E_{\text{TM(bulk)}}/N - E_{\text{TM}} \quad (2)$$

where  $E_{\text{TM(bulk)}}$  is the total energy of a TM bulk, and  $N$  is the number of atoms in the bulk.

In electrochemistry, the overall OER in acidic solutions can usually be:



It can be divided into the following four elementary reaction steps [38]:



where  $*$  represents an active site on the catalyst surface, and OH\*, O\* and OOH\* represent three different catalytic intermediates.

Based on these reactions, the adsorption energies of these species can be obtained by the following expressions:

$$\Delta E_{\text{OH}^*} = E_{\text{OH}^*} - E_* - (E_{\text{H}_2\text{O}} - 1/2E_{\text{H}_2}) \quad (5)$$

$$\Delta E_{\text{O}^*} = E_{\text{O}^*} - E_* - (E_{\text{H}_2\text{O}} - E_{\text{H}_2}) \quad (6)$$

$$\Delta E_{\text{OOH}^*} = E_{\text{OOH}^*} - E_* - (2E_{\text{H}_2\text{O}} - 3/2E_{\text{H}_2}) \quad (7)$$

where the  $E_*$ ,  $E_{\text{OH}^*}$ ,  $E_{\text{O}^*}$  and  $E_{\text{OOH}^*}$  are the total energies of the catalyst substrate without and with the adsorption of OH, O or OOH, respectively;  $E_{\text{H}_2\text{O}}$  and  $E_{\text{H}_2}$  are total energies of free H<sub>2</sub>O and H<sub>2</sub> molecules in the gas phase, respectively.

The change in free energy  $\Delta G$  can be obtained by the following expression:

$$\Delta G = \Delta E + \Delta ZPE - T\Delta S + \Delta G_U + \Delta G_{pH} \quad (8)$$

where  $\Delta E$  is the adsorption energy for the relevant intermediates involving OH, O and OOH.  $\Delta ZPE$  and  $\Delta S$  are the zero-point energy change and the change in entropy, respectively.  $\Delta G_U = -eU$ , where  $U$  is the electrode potential related to the standard hydrogen electrode.  $\Delta G_{pH} = k_B T \ln^{10} \times pH$  is the correction for Gibbs free energy depending on the concentration of  $H^+$  ions, and  $pH = 0$  was used in this study. The free energy  $G_{(H^+ + e^-)}$  is approximated with  $1/2G_{H_2}$  for each elementary step involving the proton–electron pair. The free energy of  $O_2$  can be obtained from the reaction  $2H_2O \rightarrow O_2 + 2H_2$ , for which the free energy change is 4.92 eV.

Finally, the overpotential ( $\eta$ ) of OER can be evaluated by the following formula:

$$\eta = \max\{\Delta G_a, \Delta G_b, \Delta G_c, \Delta G_d\}/e - 1.23 \text{ V} \quad (9)$$

### 3. Results and Discussion

#### 3.1. Geometric Structure, Stability and Electronic Properties for TM@C<sub>3</sub>N<sub>2</sub>

A pristine pc-C<sub>3</sub>N<sub>2</sub> monolayer belongs to the P4/MMM group, which can be considered an extended 2D network consisting of the cavities surrounded by four N atoms in pyrrole-like units or four N atoms connecting the pyrrole-like units (Figure 1a). This unique structure can make it act as a macrocyclic ligand to construct an SAC structure with TMN<sub>4</sub> units by doping TM atoms. The optimized lattice constant of a unit cell for pc-C<sub>3</sub>N<sub>2</sub> is  $a = b = 8.29 \text{ \AA}$ , which is consistent with previous results [27,28]. From Figure 1a, we can also find that there are two kinds of holes with different sizes in the pc-C<sub>3</sub>N<sub>2</sub> monolayer, namely, one is the large hole surrounded by four N atoms connecting the pyrrole-like units (marked by L), and the other is the small hole surrounded by four N atoms from the pyrrole-like units (marked by S). Such holes with different sizes will be conducive to matching TM atoms with different atomic radii, and it is highly anticipated that the highly active centers of OER can be realized in the pc-C<sub>3</sub>N<sub>2</sub> monolayer. In addition, the calculated density of states (DOS) results reveal that the pristine pc-C<sub>3</sub>N<sub>2</sub> monolayer can exhibit the metallic characteristics (Figure 1b), indicating good conductivity.

Subsequently, we investigated the geometric structures, stability and electronic properties of the doped pc-C<sub>3</sub>N<sub>2</sub> systems, where the transition metal atoms in group VIII (TM = Fe, Co, Ni, Ru, Rh, Pd, Os, Ir and Pt) are used to embed into each large or small cavity (Figure 1c,d). For convenience, all these newly formed systems can be represented as TM@C<sub>3</sub>N<sub>2</sub>. After optimization, these TM@C<sub>3</sub>N<sub>2</sub> systems can still maintain a planar structure with P4/MMM symmetry, where the TM atoms are located at the center of each hole, independent of the hole size. The calculated lattice parameters are in the range of 16.244–16.505 Å, which can be very close to that of the pristine pc-C<sub>3</sub>N<sub>2</sub> ( $a = b = 16.580 \text{ \AA}$ ), indicating a large structural rigidity. As shown in Table 1, the calculated TM–N bond lengths in the large cavity (2.294–2.409 Å) can be slightly longer than those in the small cavity (1.889–1.981 Å), but all of them can also be close to the corresponding TM–N bond length of experimentally obtained metal nitrides (1.830–2.300 Å). As a result, the TM atoms may be stably anchored in these cavities of the pc-C<sub>3</sub>N<sub>2</sub> monolayer to form two different kinds of TMN<sub>4</sub> units, which can be reflected by their large positive binding energies ( $E_b$ ) in the range of 5.17–13.00 eV, as shown in Figure 1e. Besides, it has been widely accepted that a ratio of binding energy to cohesive energy ( $-E_b/E_c$ ) greater than 0.5 indicates that single atoms tend to separate on the substrate rather than aggregate together [39–41]. For all of these TM@C<sub>3</sub>N<sub>2</sub> systems, the calculated  $-E_b/E_c$  values can be greater than 0.5 (Table S1), and even most values are greater than 1, which means that TM atoms can be anchored at the holes individually rather than clustered together.

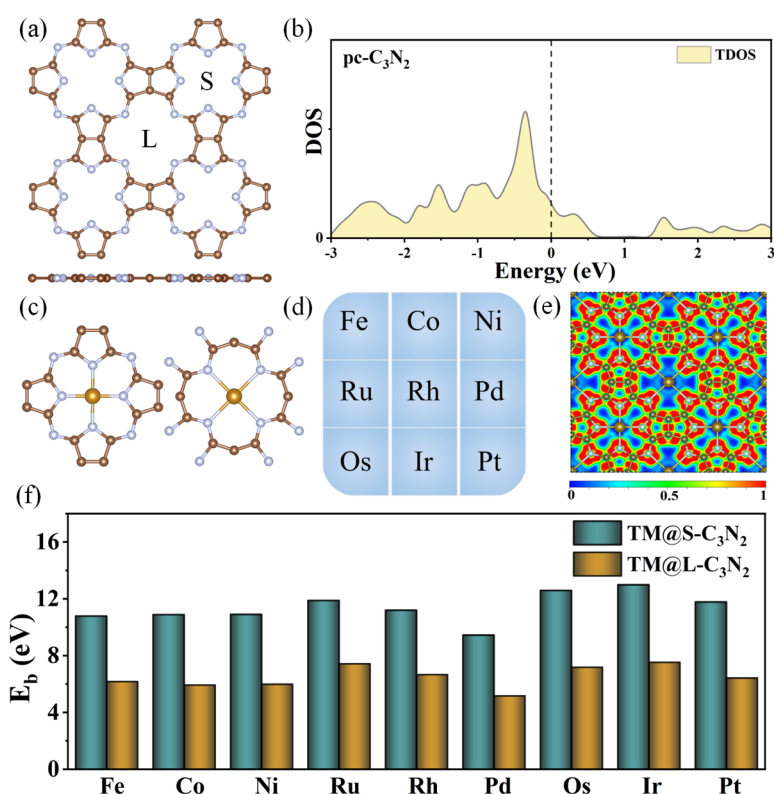


**Figure 1.** (a) Top view of the pc-C<sub>3</sub>N<sub>2</sub> monolayer. (b) Density of states (DOS) of pc-C<sub>3</sub>N<sub>2</sub>. (c) Schematic diagram of doping transition metal (TM) into the small or large cavity. (d) The group VIII TM atoms considered in the current work. (e) The electron location function for TM@C<sub>3</sub>N<sub>2</sub> systems. (f) Binding energy ( $E_b$ ) of TM atoms doped in the small (TM@S-C<sub>3</sub>N<sub>2</sub>) or large cavity (TM@L-C<sub>3</sub>N<sub>2</sub>).

**Table 1.** The calculated lattice parameters of pc-C<sub>3</sub>N<sub>2</sub> and TM@C<sub>3</sub>N<sub>2</sub> and the calculated TM-N bond lengths for TM@C<sub>3</sub>N<sub>2</sub>.

	$a = b$ (Å)	$D_{S-TM-N}$ (Å)	$D_{L-TM-N}$ (Å)
pc-C <sub>3</sub> N <sub>2</sub>	16.580	—	—
Fe@C <sub>3</sub> N <sub>2</sub>	16.345	1.914	2.356
Co@C <sub>3</sub> N <sub>2</sub>	16.385	1.952	2.333
Ni@C <sub>3</sub> N <sub>2</sub>	16.234	1.889	2.321
Ru@C <sub>3</sub> N <sub>2</sub>	16.261	1.889	2.331
Rh@C <sub>3</sub> N <sub>2</sub>	16.370	1.951	2.342
Pd@C <sub>3</sub> N <sub>2</sub>	16.300	1.942	2.294
Os@C <sub>3</sub> N <sub>2</sub>	16.244	1.891	2.323
Ir@C <sub>3</sub> N <sub>2</sub>	16.505	1.981	2.409
Pt@C <sub>3</sub> N <sub>2</sub>	16.400	1.971	2.350

Furthermore, the calculated electron location function (ELF) results reveal that all the TM-N bonds can exhibit the typical ionic bond characteristics, in view of the significant difference in ELF between the area around the TM (near to zero) and the N (about 0.9) atoms (Figure 1e). This can be further supported by the computed Bader charge analysis, where the electron of 0.58~1.23 |e| can be transferred from TM to its adjacent N atoms. In addition, we find that all the doped systems can maintain the metallic behavior (Figure 2) and that the DOS values from TM at the Fermi level can be larger than that of the pristine pc-C<sub>3</sub>N<sub>2</sub>, indicating that the conductivity is enhanced, which is conducive to the OER catalytic performance of the material.



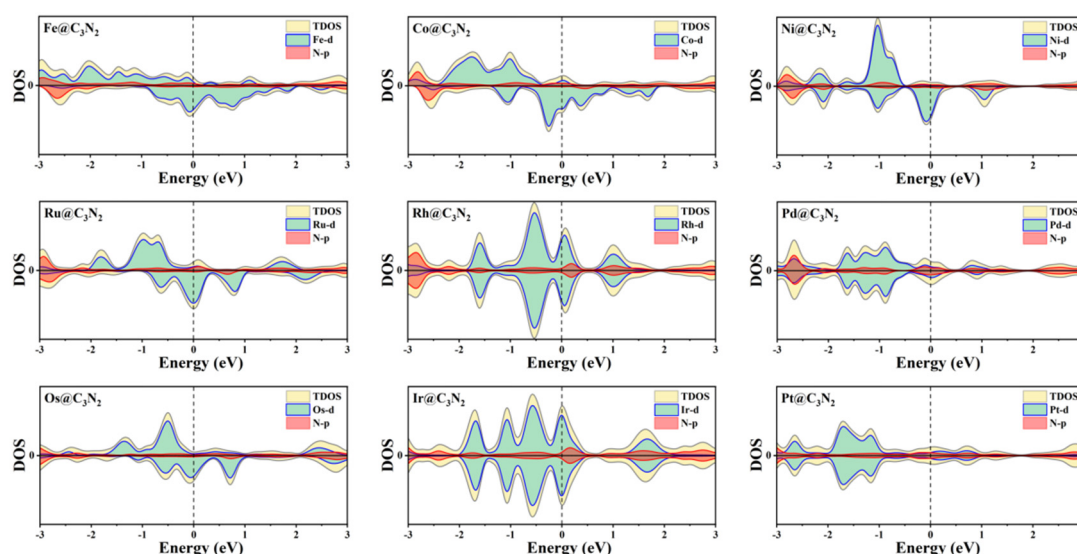


**Figure 2.** Density of states for TM@C<sub>3</sub>N<sub>2</sub> systems.

### 3.2. OER Catalytic Activity of the TM@C<sub>3</sub>N<sub>2</sub> Systems

The good stability and conductivity of these doped pc-C<sub>3</sub>N<sub>2</sub> systems containing TMN4 units can promote us to explore their potential as SAC electrocatalysts for OER in the process of water splitting. Based on these TM@C<sub>3</sub>N<sub>2</sub> structures, we systematically investigated their OER activity according to the scheme proposed by Rossmeisl et al. [38] In this method, the OER process is generally recommended to include four elementary reaction steps, each involving one proton/electron coupling transfer process, as shown in Formulas (4a)–(4d). The reaction overpotential ( $\eta$ ) can be obtained by evaluating the difference between the minimum voltages required for the four reaction steps. Herein, we will explore the OER catalytic activity of TM@C<sub>3</sub>N<sub>2</sub> systems by calculating their overpotential  $\eta$  values. By performing a computational screening of the group VIII elements (i.e., Fe, Co, Ni, Ru, Rh, Pd, Os, Ir and Pt) (Figure 1d), we find that four TM@C<sub>3</sub>N<sub>2</sub> systems doped with Co, Rh, Ir and Ru atoms can exhibit very low overpotential in the range of 0.33–0.48 V, even smaller than the state-of-the-art IrO<sub>2</sub> (0.56 V), indicating considerably high OER catalytic activity. Among them, a Rh@C<sub>3</sub>N<sub>2</sub> system can display higher OER activity due to more active sites.

Specifically, we have carried out calculations related to the OER process by adsorbing the OH, O and OOH species on the surface of TM@C<sub>3</sub>N<sub>2</sub>, where the TM atoms in small or large cavities are used as possible adsorption sites. For convenience, these different adsorption sites are labeled TM@S-C<sub>3</sub>N<sub>2</sub> and TM@L-C<sub>3</sub>N<sub>2</sub>, respectively, according to the size of the embedded hole.

Subsequently, when doping 4d TM atoms (i.e., Ru, Rh and Pd) into the small cavity of pc-C<sub>3</sub>N<sub>2</sub>, a similar situation can be observed (Figure 3d–f). To be specific, with the increase in the outer electrons of the 4d TM atoms, the overpotential  $\eta$  of TM@S-C<sub>3</sub>N<sub>2</sub> can also decrease sharply and then increase, and Rh@S-C<sub>3</sub>N<sub>2</sub> (0.33 V) can exhibit much lower overpotential than Ru@S-C<sub>3</sub>N<sub>2</sub> (1.22 V) and Pd@S-C<sub>3</sub>N<sub>2</sub> (1.35 V). Obviously, high OER catalytic activity can also be achieved by doping Rh atoms with the same number of outer electron as Co atoms.

Similarly, doping a 5d transition metal Ir atom (0.89 V), which has the same number of outer electrons as Co and Rh atoms, can also induce lower overpotential than the parallel 5d TM atoms including Os (1.50 V) and Pt (1.29 V), as shown in Figure 3g–j. Clearly, when embedding the TM atoms of group VIII into the small cavity of pc-C<sub>3</sub>N<sub>2</sub>, the number of outer electrons can play an important role in determining the overpotential value of TM@S-C<sub>3</sub>N<sub>2</sub>. Employing TM atoms (Co, Rh and Ir) with nine outer electrons can produce a lower overpotential compared with other corresponding TM atoms in the same period (Figure 4). However, we can also find that the doping of Ir can lead to a relatively larger

overpotential than Co and Rh in the same column, indicating that the periodic number of doped TM atoms also has an important influence on the overpotential, which can also be observed in the other two series (i.e., Fe/Rh/Os and Ni/Pd/Pt), as shown in Figure 4. Clearly, selecting a TM atom of group VIII in the appropriate period to match the hole size in pc-C<sub>3</sub>N<sub>2</sub> can be advantageous for realizing the high OER catalytic activity.

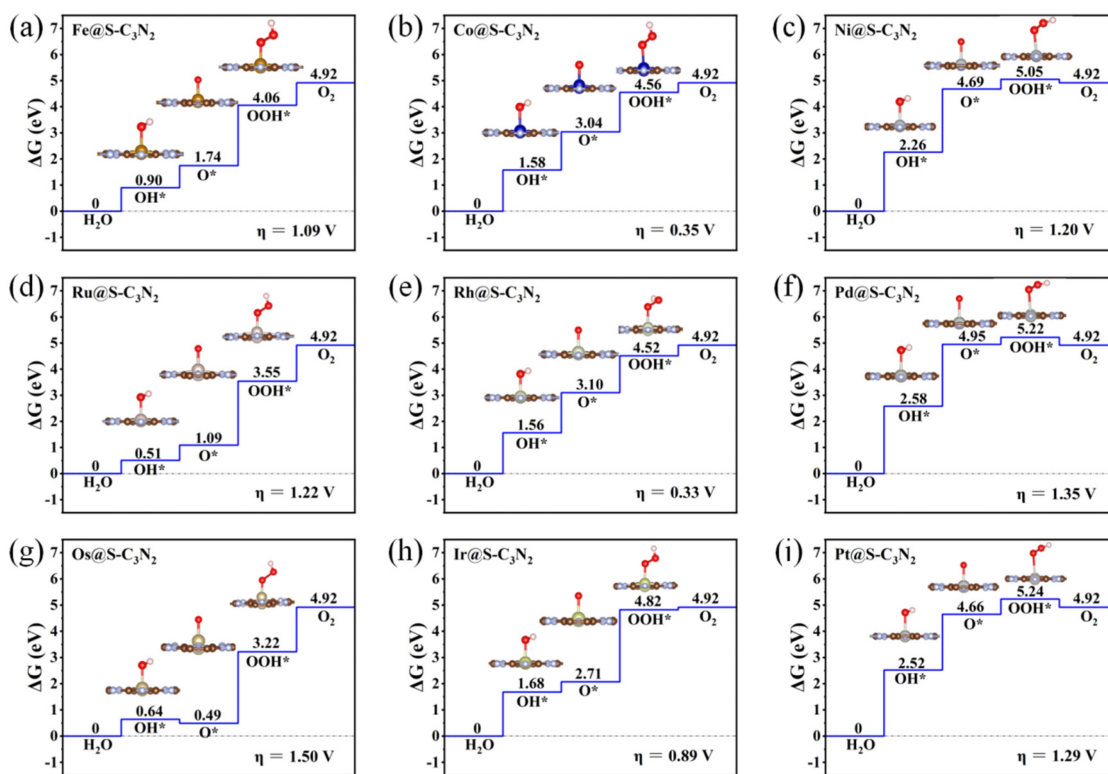


**Figure 3.** Gibbs free energy diagram of OER for the TM@S-C<sub>3</sub>N<sub>2</sub> series including Fe@S-C<sub>3</sub>N<sub>2</sub> (a), Co@S-C<sub>3</sub>N<sub>2</sub> (b), Ni@S-C<sub>3</sub>N<sub>2</sub> (c), Ru@S-C<sub>3</sub>N<sub>2</sub> (d), Rh@S-C<sub>3</sub>N<sub>2</sub> (e), Pd@S-C<sub>3</sub>N<sub>2</sub> (f), Os@S-C<sub>3</sub>N<sub>2</sub> (g), Ir@S-C<sub>3</sub>N<sub>2</sub> (h) and Pt@S-C<sub>3</sub>N<sub>2</sub> (i).

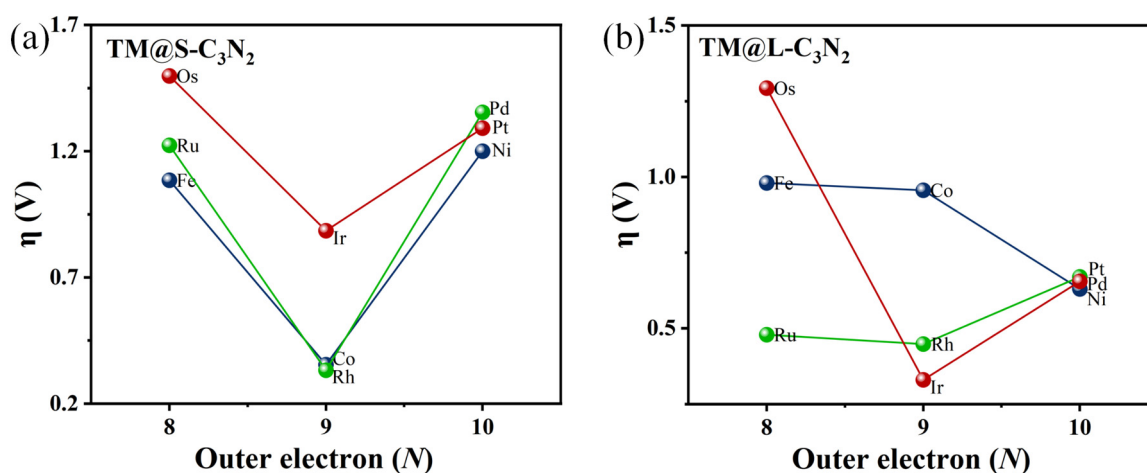


**Figure 4.** The relationships of  $\eta$  vs. outer electron (N) of TM for TM@S-C<sub>3</sub>N<sub>2</sub> (a) and TM@L-C<sub>3</sub>N<sub>2</sub> (b).

Overall, the number of outer electrons and the periodic number for the doped TM atoms can be considered two key factors to achieve high OER catalytic activity in 2D pc-C<sub>3</sub>N<sub>2</sub>, which can also be well reflected in the results of subsequently doping the group VIII TM atoms into the large cavity of pc-C<sub>3</sub>N<sub>2</sub>.

Specifically, when embedding the 5d transition metal Ir atom in the high period into the large cavity of pc-C<sub>3</sub>N<sub>2</sub>, the overpotential of Ir@L-C<sub>3</sub>N<sub>2</sub> can be significantly decreased to 0.33 V, far less than the corresponding Ir@S-C<sub>3</sub>N<sub>2</sub> (0.89 V), indicating excellent OER catalytic activity (Figure 5). However, when doping 3d transition metal Co atom in the low period, the formed Co@L-C<sub>3</sub>N<sub>2</sub> (0.96 V) displays much higher overpotential than Co@S-C<sub>3</sub>N<sub>2</sub> (0.35 V), suggesting the inert OER activity (Figure 5). Obviously, the matching between the doped TM atoms and the pore size can have an important influence on the OER catalytic activity of these SAC systems with the rigid ligand. Indeed, when a 4d transition metal Rh atom in the middle period is introduced, it can not only match the small hole size in pc-C<sub>3</sub>N<sub>2</sub> but also match the large hole size. As a result, Rh@S-C<sub>3</sub>N<sub>2</sub> (0.33 V) and Rh@L-C<sub>3</sub>N<sub>2</sub> (0.45 V) can uniformly exhibit very low overpotential (Figures 4 and 5), reflecting considerably high OER catalytic activity. In view of the formation of more active sites, the Rh-doped pc-C<sub>3</sub>N<sub>2</sub> system can exhibit the best OER catalytic performance in these doped systems with group VIII elements. In addition, different from the adsorption in the small cavity, the Ru atom anchored at the large cavity in pc-C<sub>3</sub>N<sub>2</sub> can have very low overpotential (0.48 V), presenting high OER catalytic activity.

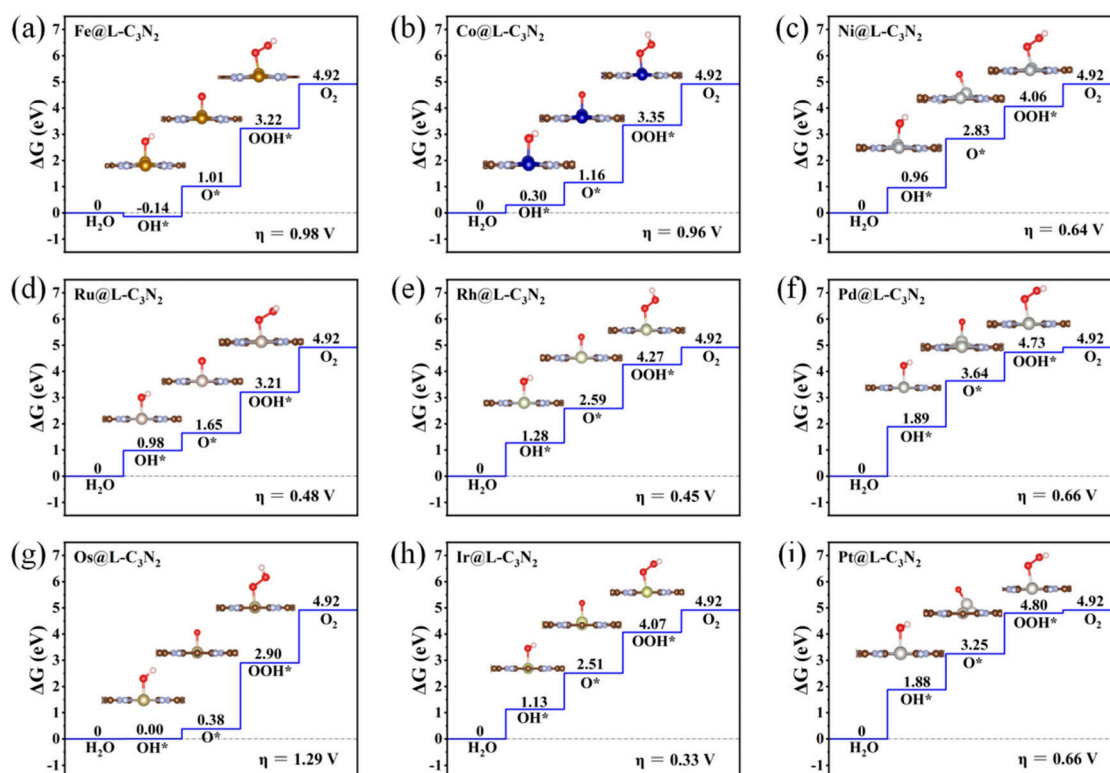


**Figure 5.** Gibbs free energy diagram of OER for TM@L-C<sub>3</sub>N<sub>2</sub> series including Fe@L-C<sub>3</sub>N<sub>2</sub> (a), Co@L-C<sub>3</sub>N<sub>2</sub> (b), Ni@L-C<sub>3</sub>N<sub>2</sub> (c), Ru@L-C<sub>3</sub>N<sub>2</sub> (d), Rh@L-C<sub>3</sub>N<sub>2</sub> (e), Pd@L-C<sub>3</sub>N<sub>2</sub> (f), Os@L-C<sub>3</sub>N<sub>2</sub> (g), Ir@L-C<sub>3</sub>N<sub>2</sub> (h) and Pt@L-C<sub>3</sub>N<sub>2</sub> (i).

Obviously, doping group VIII atoms into a pc-C<sub>3</sub>N<sub>2</sub> monolayer (for example, introducing Co/Rh into the small cavity or Ru/Rh/Ir into the large cavity) can be considered an effective strategy to realize high-efficiency SAC catalysts for OER. In particular, by embedding Rh atoms into a pc-C<sub>3</sub>N<sub>2</sub> monolayer, higher OER catalytic performance can be achieved because more active sites are produced.

### 3.3. Mechanism Analysis of OER

To understand the reasons behind the high OER catalytic activity of some TM@C<sub>3</sub>N<sub>2</sub> systems, we further performed a detailed mechanism analysis. First, we clarified the scaling relationships of ΔG<sub>O\*</sub> vs. ΔG<sub>OOH\*</sub> and ΔG<sub>O\*</sub> vs. ΔG<sub>OH\*</sub> for the two adsorption sites



corresponding to the TM atom located at the small (TM@S-C<sub>3</sub>N<sub>2</sub>) and large (TM@L-C<sub>3</sub>N<sub>2</sub>) cavities, respectively. From Figure 6, it is found that both the  $\Delta G_{\text{OH}^*}$  and  $\Delta G_{\text{OOH}^*}$  values can be linearly proportional to  $\Delta G_{\text{O}^*}$  uniformly, regardless of the size of the embedded hole in pc-C<sub>3</sub>N<sub>2</sub>. These good linear relationships can be expressed as  $\Delta G_{\text{OH}^*} = 0.47\Delta G_{\text{O}^*} + 0.20$  (correlation coefficients  $R = 0.98$ ) and  $\Delta G_{\text{OOH}^*} = 0.43\Delta G_{\text{O}^*} + 3.20$  ( $R = 0.96$ ) for the TM@S-C<sub>3</sub>N<sub>2</sub> site and  $\Delta G_{\text{OH}^*} = 0.63\Delta G_{\text{O}^*} - 0.40$  ( $R = 0.93$ ) and  $\Delta G_{\text{OOH}^*} = 0.61\Delta G_{\text{O}^*} + 2.57$  ( $R = 0.96$ ) for the TM@L-C<sub>3</sub>N<sub>2</sub> site, respectively. Therefore,  $\Delta G_{\text{O}^*}$  can be used as a valid descriptor related to the overpotential value ( $\eta$ ), which can be also reflected by the volcano curve between  $\Delta G_{\text{O}^*}$  and  $\eta$ , as shown in Figure 7.

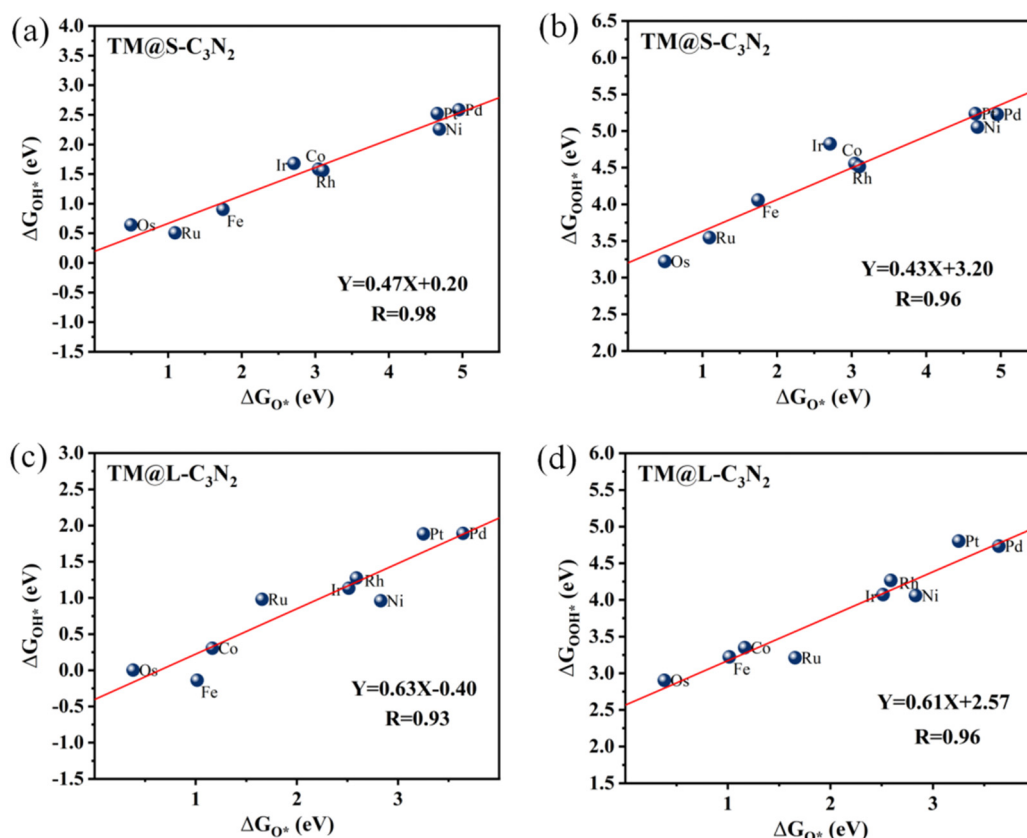


**Figure 6.** The scaling relationships corresponding to  $\Delta G_{\text{O}^*}$  vs.  $\Delta G_{\text{OOH}^*}$  and  $\Delta G_{\text{O}^*}$  vs.  $\Delta G_{\text{OH}^*}$  for TM@S-C<sub>3</sub>N<sub>2</sub> (a,b) and TM@L-C<sub>3</sub>N<sub>2</sub> (c,d).

Initially, we focus on TM@S-C<sub>3</sub>N<sub>2</sub> systems in which group VIII atoms are doped into the small cavity. Specifically, we can find from Figure 7a that, when Fe, Ru and Os atoms doped in the small hole are used as adsorption sites (TM@S-C<sub>3</sub>N<sub>2</sub>), they can be located on the left side of the volcano curve, indicating that there is a strong interaction between O\* and these TM atoms with eight outer electrons. In contrast, when the doped Ni, Pd and Pt atoms with ten outer electrons act as adsorption centers, they can be situated at the right side of the volcano curve, suggesting a weak interaction between O\* and these TM sites. It is known that in general, the adsorption strength of reaction intermediates (such as O\*) is crucial to determine the OER activity of the catalyst. Too strong or too weak adsorption of the intermediates is unfavorable to the occurrence of a catalytic reaction, in view of the fact that the former will block the catalytic site while the latter cannot provide enough driving force to bind adsorbates [42]. Therefore, when doping the Co/Rh/Ir atoms with nine outer electrons in the middle, high OER catalytic activity can be observed, because they can bring the appropriate adsorption strength of O\*, which can be reflected by the fact that they are generally at the peak of the volcano curve.

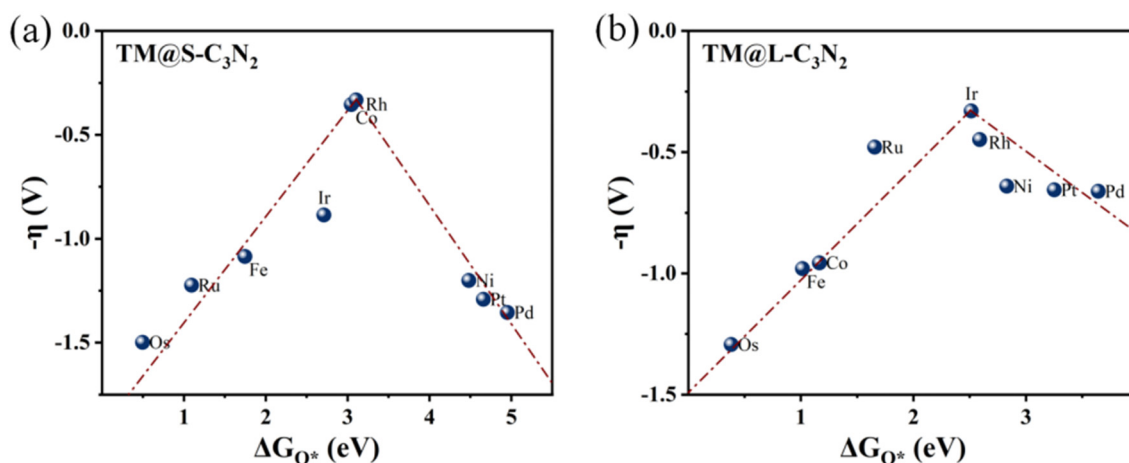
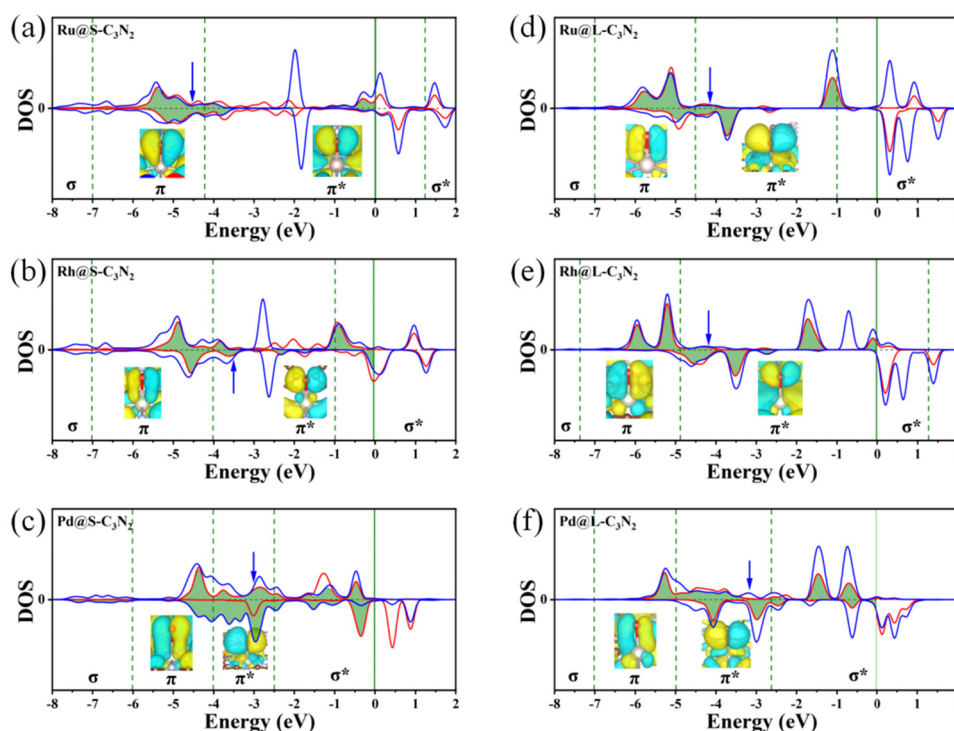


Figure 7. Volcano plots of  $-\eta$  vs.  $\Delta G_{O^*}$  for (a) TM@S-C<sub>3</sub>N<sub>2</sub> and (b) TM@L-C<sub>3</sub>N<sub>2</sub>.

To better understand that doping these TM atoms with nine outer electrons can induce the appropriate O\* adsorption state, we conduct a deep bonding analysis of the interaction between the O\* and the TM center by sampling the representative Rh@S-C<sub>3</sub>N<sub>2</sub>. For a parallel comparison, the relevant bonding analysis on the O\* adsorption of doped Ru and Pd metal centers (located on the left and right sides of the volcano curve, respectively) in the same period is also considered. As shown in Figure 8a, when the Ru with eight outer electrons serves as the adsorption site, the center of overlapping O-p and Ru-d orbitals is located in the  $\pi$  bonding area for Ru@S-C<sub>3</sub>N<sub>2</sub>, resulting in a strong interaction between the O\* and the TM center. Comparatively, when a Rh atom is introduced into the small cavity, the filling of the outer electron will increase, and the overlapping center of the O-p and Rh-d orbitals can enter the  $\pi^*$  antibonding area. The appearance of an antibonding characteristic will effectively weaken the interaction strength between the O\* and the TM center, bringing about an appropriate adsorption state of the O\* (Figure 8b). Further, when doping Pd with more outer electrons, the overlapping center of the O-p and Pd-d orbitals in the  $\pi^*$  antibonding area can continue to move towards the Fermi level, indicating an increase in antibonding characteristics (Figure 8c), which will lead to too-weak interaction between the O\* and the TM, as reflected by the large positive  $\Delta G_{O^*}$  value.

Clearly, the filling of outer electrons can play a key role in determining the high OER catalytic activity of TM@S-C<sub>3</sub>N<sub>2</sub> sites by modulating the  $\Delta G_{O^*}$  value. When doping these TM atoms into the large cavity in pc-C<sub>3</sub>N<sub>2</sub> (TM@L-C<sub>3</sub>N<sub>2</sub>), a similar situation can also be observed, that is, as the outer electron number of the TM center increases, their positions can usually change from the left side of the volcano curve to the peak and then to the right side (Figure 7b). This gradual weakening of the interaction between the O\* and the TM center can also be reasonably explained by sampling the bonding analysis of the representative Ru/Rh/Pd-doped systems. As shown in Figure 8d,f, we can find that the overlapping center of the O-p and TM-d orbitals can be located in the  $\pi^*$  bonding region and gradually approaches the Fermi level with the increase in the outer electrons, which leads to the enhancement of antibonding characteristics and the weakening of the interaction between the O\* and the TM site. In addition, unlike the case of the corresponding small cavity, when a Ru atom is doped into the large cavity in pc-C<sub>3</sub>N<sub>2</sub>, the overlapping center of the O-p and Ru-d orbitals has been located in the  $\pi^*$  bonding region (Figure 8d), which can provide an appropriate O\* adsorption state and induce high OER catalytic activity.



**Figure 8.** Partial density of states (PDOS) of the  $p$  orbitals of O atoms and the  $d$  orbitals of TM atoms after the  $O^*$  adsorption of Ru@S-C<sub>3</sub>N<sub>2</sub> (a), Rh@S-C<sub>3</sub>N<sub>2</sub> (b), Pd@S-C<sub>3</sub>N<sub>2</sub> (c), Ru@L-C<sub>3</sub>N<sub>2</sub> (d), Rh@L-C<sub>3</sub>N<sub>2</sub> (e) and Pd@L-C<sub>3</sub>N<sub>2</sub> (f). Inset: the molecular orbitals of O atom adsorbed at the TM-site in different energy ranges marked by green dashed lines. Blue arrow represents the  $p$ - $d$  overlap center.

Finally, the limiting overpotential  $\eta$  values of the TM@S-C<sub>3</sub>N<sub>2</sub> and TM@L-C<sub>3</sub>N<sub>2</sub> sites are evaluated by constructing the two-dimensional volcano diagram according to the linear relationships from Figure 6, in which the change of free energy ( $\Delta G$ ) in each step of OER can be directly related to  $\Delta G_{O^*}$ . This method has been successfully applied in previous works [42–44]. Figure 9 shows that the volcano diagrams can be divided into three regions, which correspond to the different potential determining steps (PDSs). It can be found that the adsorption strength of  $O^*$  can effectively affect the PDS step of the OER reaction. The samples with relatively weak  $O^*$  adsorption are generally located in the PDS1 ( $H_2O \rightarrow OH^*$ ) or PDS2 ( $OH^* \rightarrow O^*$ ) area, while those with strong  $O^*$  adsorption are located in the PDS3 ( $O^* \rightarrow OOH^*$ ) area. Herein, the yellow regions in the two volcano diagrams predict the limiting overpotentials  $\eta$  of the TM@S-C<sub>3</sub>N<sub>2</sub> and TM@L-C<sub>3</sub>N<sub>2</sub> series, both of which can be as small as 0.27 V. It is worth mentioning that, in the systems we designed, the overpotentials of some active sites (such as Co@S-C<sub>3</sub>N<sub>2</sub>, Rh@S-C<sub>3</sub>N<sub>2</sub> and Ir@L-C<sub>3</sub>N<sub>2</sub>) can be as low as 0.33–0.35 V, very close to the limit value. All these findings can provide very in depth insight into the design of SAC catalysts with high OER activity under the rigid pc-C<sub>3</sub>N<sub>2</sub> framework.

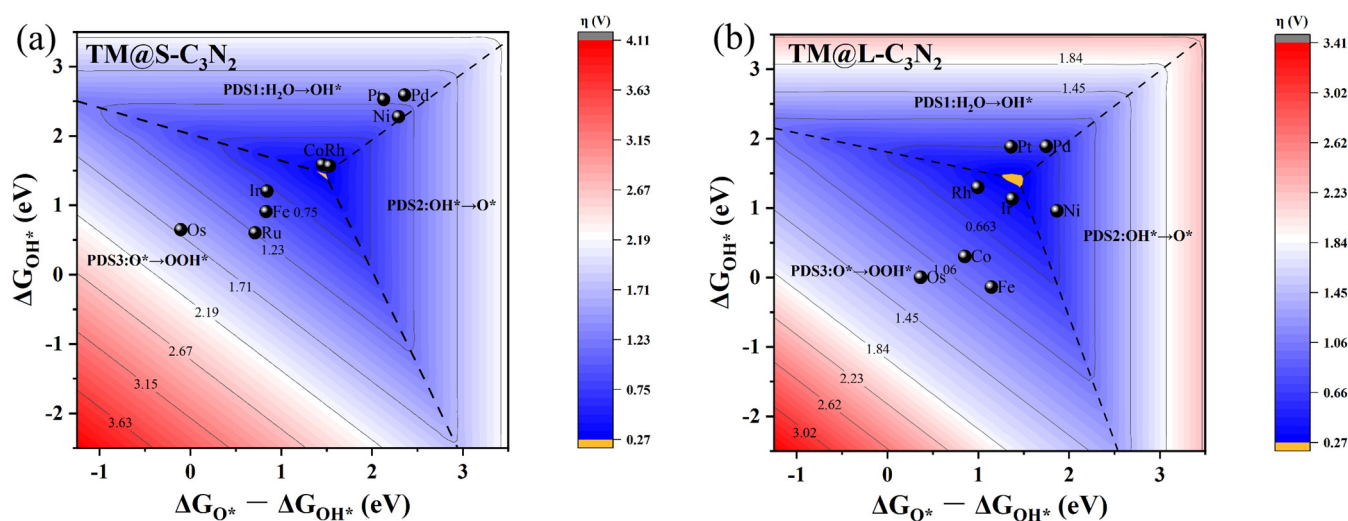


**Figure 9.** The 2D colored contour plots of OER activity volcanos for (a) TM@S-C<sub>3</sub>N<sub>2</sub> and (b) TM@L-C<sub>3</sub>N<sub>2</sub> by presenting the  $\eta$  values as a function of the Gibbs free energies.

#### 4. Conclusions

In this study, we constructed a series of two-dimensional SAC systems by doping the TM atoms of the group VIII into the cavities of a rigid pc-C<sub>3</sub>N<sub>2</sub> monolayer and systematically investigate their structures and OER catalytic performance based on the DFT calculations. The following intriguing findings can be obtained:

- (1) All these TM@C<sub>3</sub>N<sub>2</sub> systems can exhibit high structural stability, wherein the TM atoms are stably anchored in small and large cavities of a pc-C<sub>3</sub>N<sub>2</sub> monolayer to form two different kinds of TMN<sub>4</sub> units. Compared with the pristine pc-C<sub>3</sub>N<sub>2</sub> with metallic characteristics, the conductivity of these doped systems can be further enhanced. All these advantages are conducive to the OER catalytic performance of the materials.
- (2) Through a calculation screening of the TM atoms in group VIII, it is found that four new TM@C<sub>3</sub>N<sub>2</sub> systems doped with Co/Rh/Ir/Ru atoms can possess very low overpotential (0.33~0.48 V), indicating the considerably high OER catalytic activity, where the adsorption sites including Co@S-C<sub>3</sub>N<sub>2</sub>, Rh@S-C<sub>3</sub>N<sub>2</sub>, Ru@L-C<sub>3</sub>N<sub>2</sub>, Rh@L-C<sub>3</sub>N<sub>2</sub> and Ir@L-C<sub>3</sub>N<sub>2</sub> can be used as the active sites. As a result, the Rh@C<sub>3</sub>N<sub>2</sub> system can exhibit higher OER catalytic performance, due to the higher density of active sites.
- (3) It is found that  $\Delta G_{O^*}$  can be used as an effective descriptor of the OER catalytic activity of TM@C<sub>3</sub>N<sub>2</sub> systems. The number of outer electrons, the periodic number of doped TM atoms and the cavity size can be the crucial factors in determining the  $\Delta G_{O^*}$  value, and the effective cooperation between them can lead to moderate  $\Delta G_{O^*}$  values, bringing about excellent OER catalytic performance in these SAC catalysts.

Obviously, introducing group VIII atoms with nine outer electrons into the cavities of a rigid pc-C<sub>3</sub>N<sub>2</sub> ligand can be considered an effective strategy to realize SAC catalysts with high OER catalytic performance. All these fascinating findings are conducive to the design of new and efficient OER catalysts.

**Supplementary Materials:** The following supporting information can be downloaded at: <https://www.mdpi.com/article/10.3390/molecules28010254/s1>, Figure S1: Gibbs free energy diagram of OER in solvation condition for Ir@S-C<sub>3</sub>N<sub>2</sub>(a) and Ir@L-C<sub>3</sub>N<sub>2</sub>(b); Figure S2: Gibbs free energy diagram of OER for Co@C<sub>3</sub>N<sub>2</sub> under the DFT+U method; Table S1: The binding energy  $E_b$  (eV), cohesive energy  $E_c$  (eV), and the ratio of  $-E_b/E_c$  for the studied systems.

**Author Contributions:** Investigation, data curation, writing—original draft preparation, Q.W.; visualization, methodology, E.Y., R.L. and M.L.; formal analysis, resources, W.Z.; conceptualization, investigation, writing—review and editing, supervision, project administration, funding acquisition, G.Y. and W.C. All authors have read and agreed to the published version of the manuscript.

**Funding:** This work was financially supported by the National Natural Science Foundation of China (21673094 and 21673093), the Natural Science Foundation of Fujian Province (2020J01147 and 2022J01167), Research Foundation of Academy of Carbon Neutrality of Fujian Normal University (TZH2022-05), Minjiang Scholar and startup fund for high-level talent at Fujian Normal University, Program for Innovative Research Team in Science and Technology in Fujian Province University and Fujian-Taiwan Science and Technology Cooperation Base of Biomedical Materials and Tissue Engineering (2021D039).

**Institutional Review Board Statement:** Not applicable.

**Informed Consent Statement:** Not applicable.

**Data Availability Statement:** Not applicable.

**Acknowledgments:** We acknowledge the Computing Center of Jilin Province and the High Performance Computing Center (HPCC) of Jilin University for supercomputer time.

**Conflicts of Interest:** The authors declare no conflict of interest.

**Sample Availability:** Samples are available from the authors.

## References

- Panwar, N.L.; Kaushik, S.C.; Kothari, S. Role of renewable energy sources in environmental protection: A review. *Renew. Sustain. Energy Rev.* **2011**, *15*, 1513–1524. [\[CrossRef\]](#)
- Liu, Z. Clean Energy Replacement and Electricity Replacement. In *Global Energy Interconnection*; Academic Press: Boston, MA, USA, 2015; pp. 65–90. [\[CrossRef\]](#)
- Abe, J.O.; Popoola, A.P.I.; Ajenifuja, E.; Popoola, O.M. Hydrogen energy, economy and storage: Review and recommendation. *Int. J. Hydrog. Energy* **2019**, *44*, 15072–15086. [\[CrossRef\]](#)
- Midilli, A.; Ay, M.; Dincer, I.; Rosen, M.A. On hydrogen and hydrogen energy strategies. *Renew. Sustain. Energy Rev.* **2005**, *9*, 255–271. [\[CrossRef\]](#)
- Ursua, A.; Gandia, L.M.; Sanchis, P. Hydrogen Production From Water Electrolysis: Current Status and Future Trends. *Proc. IEEE* **2012**, *100*, 410–426. [\[CrossRef\]](#)
- Anwar, S.; Khan, F.; Zhang, Y.; Djire, A. Recent development in electrocatalysts for hydrogen production through water electrolysis. *Int. J. Hydrog. Energy* **2021**, *46*, 32284–32317. [\[CrossRef\]](#)
- Mo, J.; Kang, Z.; Yang, G.; Li, Y.; Retterer, S.T.; Cullen, D.A.; Toops, T.J.; Bender, G.; Pivovar, B.S.; Green, J.B., Jr.; et al. In situ investigation on ultrafast oxygen evolution reactions of water splitting in proton exchange membrane electrolyzer cells. *J. Mater. Chem. A* **2017**, *5*, 18469–18475. [\[CrossRef\]](#)
- Zhou, Y.; Chen, L.; Sheng, L.; Luo, Q.; Zhang, W.; Yang, J. Dual-metal atoms embedded into two-dimensional covalent organic framework as efficient electrocatalysts for oxygen evolution reaction: A DFT study. *Nano Res.* **2022**, *15*, 7994–8000. [\[CrossRef\]](#)
- Lee, Y.; Suntivich, J.; May, K.J.; Perry, E.E.; Shao-Horn, Y. Synthesis and Activities of Rutile IrO<sub>2</sub> and RuO<sub>2</sub> Nanoparticles for Oxygen Evolution in Acid and Alkaline Solutions. *J. Phys. Chem. Lett.* **2012**, *3*, 399–404. [\[CrossRef\]](#)
- McCrory, C.C.; Jung, S.; Peters, J.C.; Jaramillo, T.F. Benchmarking heterogeneous electrocatalysts for the oxygen evolution reaction. *J. Am. Chem. Soc.* **2013**, *135*, 16977–16987. [\[CrossRef\]](#)
- Jian, J.; Chen, W.; Zeng, D.; Chang, L.; Zhang, R.; Jiang, M.; Yu, G.; Huang, X.; Yuan, H.; Feng, S. Metal-ionic-conductor potassium ferrite nanocrystals with intrinsic superhydrophilic surfaces for electrocatalytic water splitting at ultrahigh current densities. *J. Mater. Chem. A* **2021**, *9*, 7586–7593. [\[CrossRef\]](#)
- Feng, T.; Yu, G.; Tao, S.; Zhu, S.; Ku, R.; Zhang, R.; Zeng, Q.; Yang, M.; Chen, Y.; Chen, W.; et al. A highly efficient overall water splitting ruthenium-cobalt alloy electrocatalyst across a wide pH range via electronic coupling with carbon dots. *J. Mater. Chem. A* **2020**, *8*, 9638–9645. [\[CrossRef\]](#)
- Yang, L.; Yu, G.; Ai, X.; Yan, W.; Duan, H.; Chen, W.; Li, X.; Wang, T.; Zhang, C.; Huang, X.; et al. Efficient oxygen evolution electrocatalysis in acid by a perovskite with face-sharing IrO<sub>6</sub> octahedral dimers. *Nat. Commun.* **2018**, *9*, 5236. [\[CrossRef\]](#) [\[PubMed\]](#)
- Qian, G.; Yu, G.; Lu, J.; Luo, L.; Wang, T.; Zhang, C.; Ku, R.; Yin, S.; Chen, W.; Mu, S. Ultra-thin N-doped-graphene encapsulated Ni nanoparticles coupled with MoO<sub>2</sub> nanosheets for highly efficient water splitting at large current density. *J. Mater. Chem. A* **2020**, *8*, 14545–14554. [\[CrossRef\]](#)
- Li, C.; Yu, G.; Shen, X.; Li, Y.; Chen, W. Theoretical Study on the High HER/OER Electrocatalytic Activities of 2D GeSi, SnSi, and SnGe Monolayers and Further Improvement by Imposing Biaxial Strain or Doping Heteroatoms. *Molecules* **2022**, *27*, 5092. [\[CrossRef\]](#)
- Lin, Y.; Tian, Z.; Zhang, L.; Ma, J.; Jiang, Z.; Deibert, B.J.; Ge, R.; Chen, L. Chromium-ruthenium oxide solid solution electrocatalyst for highly efficient oxygen evolution reaction in acidic media. *Nat. Commun.* **2019**, *10*, 162. [\[CrossRef\]](#)
- Liu, J.; Zhang, J.; Zhou, H.; Liu, B.; Dong, H.; Lin, X.; Qin, Y. Lignin-derived carbon-supported MoC-FeNi heterostructure as efficient electrocatalysts for oxygen evolution reaction. *J. Colloid Interface Sci.* **2022**, *629*, 822–831. [\[CrossRef\]](#)



18. Zhu, K.; Shi, F.; Zhu, X.; Yang, W. The roles of oxygen vacancies in electrocatalytic oxygen evolution reaction. *Nano Energy* **2020**, *73*, 104761. [\[CrossRef\]](#)
19. Song, S.; Wang, Y.; Davis, R.C.; Ren, Z.; Xiao, X.; Yang, G.; Wang, D.; Bao, J.; Zhang, Q.; Chen, S.; et al. Electrochemical Insight into  $\text{Na}_x\text{CoO}_2$  for the Oxygen Evolution Reaction and the Oxygen Reduction Reaction. *Chem. Mater.* **2021**, *33*, 6299–6310. [\[CrossRef\]](#)
20. Kwon, Y.; Kim, T.Y.; Kwon, G.; Yi, J.; Lee, H. Selective Activation of Methane on Single-Atom Catalyst of Rhodium Dispersed on Zirconia for Direct Conversion. *J. Am. Chem. Soc.* **2017**, *139*, 17694–17699. [\[CrossRef\]](#)
21. Li, J.; Guan, Q.; Wu, H.; Liu, W.; Lin, Y.; Sun, Z.; Ye, X.; Zheng, X.; Pan, H.; Zhu, J.; et al. Highly Active and Stable Metal Single-Atom Catalysts Achieved by Strong Electronic Metal-Support Interactions. *J. Am. Chem. Soc.* **2019**, *141*, 14515–14519. [\[CrossRef\]](#)
22. Wang, Y.; Tang, Y.J.; Zhou, K. Self-Adjusting Activity Induced by Intrinsic Reaction Intermediate in Fe-N-C Single-Atom Catalysts. *J. Am. Chem. Soc.* **2019**, *141*, 14115–14119. [\[CrossRef\]](#)
23. Zhang, J.; Zhao, Y.; Chen, C.; Huang, Y.C.; Dong, C.L.; Chen, C.J.; Liu, R.S.; Wang, C.; Yan, K.; Li, Y.; et al. Tuning the Coordination Environment in Single-Atom Catalysts to Achieve Highly Efficient Oxygen Reduction Reactions. *J. Am. Chem. Soc.* **2019**, *141*, 20118–20126. [\[CrossRef\]](#) [\[PubMed\]](#)
24. Zhang, L.; Jia, Y.; Gao, G.; Yan, X.; Chen, N.; Chen, J.; Soo, M.T.; Wood, B.; Yang, D.; Du, A.; et al. Graphene Defects Trap Atomic Ni Species for Hydrogen and Oxygen Evolution Reactions. *Chem* **2018**, *4*, 285–297. [\[CrossRef\]](#)
25. Lin, C.; Zhao, Y.; Zhang, H.; Xie, S.; Li, Y.F.; Li, X.; Jiang, Z.; Liu, Z.P. Accelerated active phase transformation of NiO powered by Pt single atoms for enhanced oxygen evolution reaction. *Chem. Sci.* **2018**, *9*, 6803–6812. [\[CrossRef\]](#) [\[PubMed\]](#)
26. Chen, Z.; Fan, X.; Shen, Z.; Ruan, X.; Wang, L.; Zeng, H.; Wang, J.; An, Y.; Hu, Y. Cu Anchored  $\text{Ti}_2\text{NO}_2$  as High Performance Electrocatalyst for Oxygen Evolution Reaction: A Density Functional Theory Study. *ChemCatChem* **2020**, *12*, 4059–4066. [\[CrossRef\]](#)
27. Tsetseris, L. Phthalo-carbonitride: An ab initio prediction of a stable two-dimensional material. *2d Mater.* **2016**, *3*, 021006. [\[CrossRef\]](#)
28. Xu, W.; Kang, X.; Duan, X. Phthalo-carbonitride nanosheets as excellent  $\text{N}_2$  reduction reaction electrocatalysts: A first-principles study. *Phys. Chem. Chem. Phys.* **2022**, *24*, 14472–14478. [\[CrossRef\]](#)
29. Kresse, G.; Hafner, J. Ab initio molecular dynamics for liquid metals. *Phys. Rev. B Condens. Matter* **1993**, *47*, 558–561. [\[CrossRef\]](#)
30. Vanderbilt, D. Soft self-consistent pseudopotentials in a generalized eigenvalue formalism. *Phys. Rev. B Condens. Matter* **1990**, *41*, 7892–7895. [\[CrossRef\]](#)
31. Kresse, G.; Joubert, D. From ultrasoft pseudopotentials to the projector augmented-wave method. *Phys. Rev. B* **1999**, *59*, 1758. [\[CrossRef\]](#)
32. Blochl, P.E. Projector augmented-wave method. *Phys. Rev. B Condens. Matter* **1994**, *50*, 17953–17979. [\[CrossRef\]](#) [\[PubMed\]](#)
33. Perdew, J.P.; Burke, K.; Ernzerhof, M. Generalized gradient approximation made simple. *Phys. Rev. Lett.* **1996**, *77*, 3865. [\[CrossRef\]](#) [\[PubMed\]](#)
34. Grimme, S. Semiempirical GGA-type density functional constructed with a long-range dispersion correction. *J. Comput. Chem.* **2006**, *27*, 1787–1799. [\[CrossRef\]](#)
35. Kresse, G.; Hafner, J. Ab initio molecular-dynamics simulation of the liquid-metal-amorphous-semiconductor transition in germanium. *Phys. Rev. B Condens. Matter* **1994**, *49*, 14251–14269. [\[CrossRef\]](#)
36. Monkhorst, H.J.; Pack, J.D. Special points for Brillouin-zone integrations. *Phys. Rev. B* **1976**, *13*, 5188–5192. [\[CrossRef\]](#)
37. Ye, J.; Feng, Z.; Li, H.; Dai, X.Q. DFT+U study on the magnetic properties of 3d transition metal doped  $\beta$  borophene. *Phys. E Low-Dimens. Syst. Nanostructures* **2023**, *147*. [\[CrossRef\]](#)
38. Rossmekl, J.; Qu, Z.W.; Zhu, H.; Kroes, G.J.; Nørskov, J.K. Electrolysis of water on oxide surfaces. *J. Electroanal. Chem.* **2007**, *607*, 83–89. [\[CrossRef\]](#)
39. Liu, X.; Hupalo, M.; Wang, C.-Z.; Lu, W.-C.; Thiel, P.A.; Ho, K.-M.; Tringides, M.C. Growth morphology and thermal stability of metal islands on graphene. *Phys. Rev. B* **2012**, *86*, 081414. [\[CrossRef\]](#)
40. Su, Z.; Pang, R.; Ren, X.; Li, S. Synergetic role of charge transfer and strain engineering in improving the catalysis of Pd single-atom-thick motifs stabilized on a defect-free  $\text{MoS}_2/\text{Ag}(\text{Au})(111)$  heterostructure. *J. Mater. Chem. A* **2020**, *8*, 17238–17247. [\[CrossRef\]](#)
41. Chan, K.T.; Neaton, J.B.; Cohen, M.L. First-principles study of metal adatom adsorption on graphene. *Phys. Rev. B* **2008**, *77*, 235430. [\[CrossRef\]](#)
42. Xue, Z.; Zhang, X.; Qin, J.; Liu, R. TMN4 complex embedded graphene as bifunctional electrocatalysts for high efficiency OER/ORR. *J. Energy Chem.* **2021**, *55*, 437–443. [\[CrossRef\]](#)
43. Xue, Z.; Zhang, X.; Qin, J.; Liu, R. Revealing Ni-based layered double hydroxides as high-efficiency electrocatalysts for the oxygen evolution reaction: A DFT study. *J. Mater. Chem. A* **2019**, *7*, 23091–23097. [\[CrossRef\]](#)
44. Zhang, H.; Wei, W.; Wang, S.; Wang, H.; Huang, B.; Dai, Y.  $\text{H}_4\text{4,4}$ -graphyne with double Dirac points as high-efficiency bifunctional electrocatalysts for water splitting. *J. Mater. Chem. A* **2021**, *9*, 4082–4090. [\[CrossRef\]](#)

**Disclaimer/Publisher’s Note:** The statements, opinions and data contained in all publications are solely those of the individual author(s) and contributor(s) and not of MDPI and/or the editor(s). MDPI and/or the editor(s) disclaim responsibility for any injury to people or property resulting from any ideas, methods, instructions or products referred to in the content.